Spin-dependent potentials in pure QCD on a 32^4 lattice.

I J Ford†

Department of Theoretical Physics, University of Oxford, Oxford OX1 3NP, UK

Abstract. Pure QCD is studied on a large Euclidean lattice consisting of 32^4 points at values of the coupling β equal to 6.29, 6.585 and 6.88. Results are presented for the lowest-order spin-dependent corrections to the non-relativistic potential between a quark and an antiquark. Working within a Bethe–Salpeter formalism, it is concluded that the linear term in the non-relativistic potential is consistent with having arisen from scalar exchange: the Coulomb-like term similarly arises from a purely vector exchange. As part of the above study, calculations of the A_{1u} hybrid potential in quarkonium are made, showing it to be similar in behaviour to the E_u potential.

1. Introduction

A previous paper [1] presented some of the results of a recent Monte Carlo study of pure quantum chromodynamics (QCD). The aim of the study was to gain a more thorough understanding of the properties of pure QCD by defining the theory on the largest regular spacetime lattice yet constructed, consisting of 32^4 points with periodic boundary conditions. A lattice QCD calculation requires the specification of a coupling β, which is linked with the size of the lattice spacing a [2]. The three values of β taken, 6.29, 6.585 and 6.88, correspond, respectively, to a finer and finer four-dimensional spacetime grid. The investigation is extended here to the spin dependence of the quark–antiquark potential. The fine spacing of the lattices lend themselves to the study of the short-range structure of these interactions.

An intuitive derivation of the spin–spin type potentials is given in §2. The details of the Monte Carlo calculations and the methods used to overcome the considerable computational difficulties appear in §3. Section 4 contains numerical results for the spin–spin and spin–orbit potentials describing the ground state of a heavy quark–antiquark system. This state is classified as A_{1g} under the lattice symmetry group of the q$\bar{\text{q}}$ system (see [3] for a full discussion). Calculations are also presented for the non-relativistic potential in the q$\bar{\text{q}}$ system classified as A_{1u}. This potential is important for calculating the masses of hybrid mesons [4]. The conclusions of the study are summarised in §5.

---

† Present address: Theoretical Physics Division, B424.4, Harwell Laboratory, Didcot, Oxfordshire OX11 0RA, UK.

2. Spin-dependent corrections to the central potential in quarkonium

The evaluation of expectation values of Wilson loops is the standard method on the lattice for finding the non-relativistic energy of a $q\bar{q}$ pair. The non-relativistic corrections can be found by an expansion of the quark propagators in $1/m_q$ [5], but here a more intuitive derivation is followed which emphasises the role of the relativistic terms in the $q\bar{q}$ Hamiltonian, and in lattice terms, the form of operator modelling the $q\bar{q}$ state.

The correction to the non-relativistic potential energy for the $q\bar{q}$ state $|l\rangle$ is given in second-order perturbation theory by

$$\Delta E = \sum_{n \neq l} \frac{\langle l|H'|n\rangle\langle n|H'|l\rangle}{E_l - E_n} \tag{1}$$

where $|n\rangle$ are eigenstates with energy E_n of the Euclidean non-relativistic Hamiltonian. H' is the perturbation, which for illustration is taken to be simply the chromomagnetic coupling to quark and antiquark spins

$$H' = -\boldsymbol{B}(\boldsymbol{x}).(\boldsymbol{\mu}_1 \delta^3(\boldsymbol{x} - \boldsymbol{r}_1) - \boldsymbol{\mu}_2 \delta^3(\boldsymbol{x} - \boldsymbol{r}_2)) \tag{2}$$

where $\boldsymbol{r}_1$ and $\boldsymbol{r}_2$ are the positions of the q and $\bar{q}$ respectively, $\boldsymbol{\mu}_i$ is taken to be $-g\boldsymbol{\sigma}_i/(2m_q)$, $\boldsymbol{\sigma}$ are the Pauli matrices, g is the charge and m_q the mass of the fermion. $\boldsymbol{B}$ is the chromomagnetic field operator. With this H' equation (1) becomes

$$\Delta E = -2 \, \mathrm{Re} \left(\frac{g^2}{4m_q^2} \sum_{n \neq l} \frac{1}{E_l - E_n} \langle l|\boldsymbol{\sigma}_1.\boldsymbol{B}(\boldsymbol{r}_1)|n\rangle\langle n|\boldsymbol{\sigma}_2.\boldsymbol{B}(\boldsymbol{r}_2)|l\rangle \right) \tag{3}$$

having discarded two spin-independent pieces. Equation (3) can be written, for $E_n > E_l$, as

$$\Delta E = \frac{g^2}{2m_q^2} \, \mathrm{Re} \left(\sum_{n \neq l} \int_0^\infty e^{-(E_n - E_l)t} \, \mathrm{d}t \langle l|\boldsymbol{\sigma}_1.\boldsymbol{B}(\boldsymbol{r}_1)|n\rangle\langle n|\boldsymbol{\sigma}_2.\boldsymbol{B}(\boldsymbol{r}_2)|l\rangle \right) \tag{4}$$

$$= \frac{g^2}{2m_q^2} \, \mathrm{Re} \left(\int_0^\infty \mathrm{d}t \langle l|\boldsymbol{\sigma}_1.\boldsymbol{B}(\boldsymbol{r}_1,t)\boldsymbol{\sigma}_2.\boldsymbol{B}(\boldsymbol{r}_2,0)|l\rangle \right) \tag{5}$$

since $\langle l|\boldsymbol{B}|l\rangle = 0$. Note that spin-dependent corrections to hybrid states are not included in this formalism. The state $|l\rangle$ can be represented as

$$|l\rangle = \mathrm{Lim}_{\tau \to \infty} \left(\frac{A(-\tau/2)|0\rangle}{\langle l|A|0\rangle e^{-E_l\tau/2}} \right) \tag{6}$$

where A is a quarkonium operator acting at Euclidean time $-\tau/2$ creating a q and $\bar{q}$ at $\boldsymbol{r}_1$ and $\boldsymbol{r}_2$ together with a gluonic binding field. Hence, for large enough τ

$$\Delta E = \frac{g^2}{2m_q^2} \, \mathrm{Re} \left(\int_0^{\tau/2} \mathrm{d}t \frac{\langle 0|A^\dagger(\tau/2)\sigma_1^i\sigma_2^j B_i(\boldsymbol{r}_1,t)B_j(\boldsymbol{r}_2,0)A(-\tau/2)|0\rangle}{\langle 0|A^\dagger(\tau/2)A(-\tau/2)|0\rangle} \right). \tag{7}$$

The vacuum expectation values can be interpreted easily when written as path integrals. The denominator of the integrand in (7) is a quarkonium operator correlation function over Euclidean time τ. On the lattice the numerator can be written as

$$\frac{1}{Z_{\text{LAT}}} \int \Pi \mathrm{d}U_\mu(n)\mathrm{d}\psi(n)\mathrm{d}\bar{\psi}(n)A^\dagger(\tau/2)\sigma_1^i\sigma_2^j B_i^{\text{L}}(r_1,t)B_j^{\text{L}}(r_2,0)A(-\tau/2)\mathrm{e}^{-S[U,\psi,\bar{\psi}]}$$

$$= \langle\sigma_1^i\sigma_2^j\rangle\langle B_i^{\text{L}}(r_1,t)B_j^{\text{L}}(r_2,0)\rangle_{\text{C}} \tag{8}$$

where B^{L} is a lattice representation of the chromomagnetic field operator, S is the lattice action, Z_{LAT} is the lattice representation of the vacuum generating functional, ψ and $\bar{\psi}$ are the quark and antiquark fields respectively, and U_μ are the lattice link variables. If the operators A are taken to be products of links terminating on fermion operators then, after the integration over ψ and $\bar{\psi}$, (8) becomes simply the expectation value of a Wilson loop containing insertions of chromomagnetic field components, as in figure 1. This corresponds with the results of [5], but this approach shows the generality of the spatial parts of the loop (the structure of the operator A). This is shown shaded in figure 1. The notation in (8) eliminates the (smeared) contour appearing in the expectation value; its inclusion is signified by the suffix C. The Pauli matrices in (8) appear as an expectation value in the spin part of the state created by A.
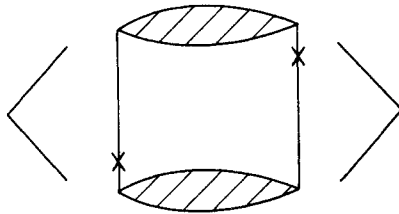
Figure 1. Representation of an expectation value of a quarkonium operator correlation function including colour field operators, represented by crosses. The shaded areas represent smeared operators.

The correction ΔE can be used to write down a spin–spin potential:

$$V_{\text{ss}} = \frac{S_1 \cdot S_2}{3m_q^2}V_4(R) + \frac{1}{m_q^2}\left(\frac{(R.S_1)(R.S_2)}{R^2} - \tfrac{1}{3}S_1.S_2\right)V_3(R) \tag{9}$$

where $S_1(S_2)$ is the spin of the quark (antiquark), $R = r_1 - r_2$, $R = |R|$, and the scalar and tensor spin–spin potentials are given, respectively, by

$$V_4(R) = \frac{g^2}{\langle 1\rangle_{\text{C}}}\int_{-\infty}^{+\infty}\mathrm{d}t\langle 2B_x^{\text{L}}(r_1,0)B_x^{\text{L}}(r_2,t) + B_z^{\text{L}}(r_1,0)B_z^{\text{L}}(r_2,t)\rangle_{\text{C}} \tag{10}$$

and

$$V_3(R) = \frac{g^2}{\langle 1\rangle_{\text{C}}}\int_{-\infty}^{+\infty}\mathrm{d}t\langle -B_x^{\text{L}}(r_1,0)B_x^{\text{L}}(r_2,t) + B_z^{\text{L}}(r_1,0)B_z^{\text{L}}(r_2,t)\rangle_{\text{C}} \tag{11}$$

when R is taken to lie in the z direction.

Now, the spin–orbit contribution to the qq̄ potential to $O(1/m_q^2)$ is

$$V_{so} = \frac{1}{2m_q^2}[(\boldsymbol{R} \times \boldsymbol{p}_1).\boldsymbol{S}_1 - (\boldsymbol{R} \times \boldsymbol{p}_2).\boldsymbol{S}_2]\left(\frac{V_0'(R)}{R} + \frac{2V_1'(R)}{R}\right)$$
$$+ \frac{1}{m_q^2}[(\boldsymbol{R} \times \boldsymbol{p}_1).\boldsymbol{S}_2 - (\boldsymbol{R} \times \boldsymbol{p}_2).\boldsymbol{S}_1]\frac{V_2'(R)}{R} \tag{12}$$

where

$$V_1'(R) = \frac{g^2}{\langle 1 \rangle_C}\int_{-\infty}^{+\infty} dt\, t\langle B_x^L(\boldsymbol{r}_1, 0)E_y^L(\boldsymbol{r}_1, t)\rangle_C \tag{13}$$

$$V_2'(R) = \frac{g^2}{\langle 1 \rangle_C}\int_{-\infty}^{+\infty} dt\, t\langle B_x^L(\boldsymbol{r}_2, 0)E_y^L(\boldsymbol{r}_1, t)\rangle_C \tag{14}$$

and $V_0(R)$ is the non-relativistic qq̄ potential. Equations (9–14) are derived with greater rigour in [5], but the derivation for $V_{3,4}$ above illustrates the conditions necessary for a successful lattice calculation. The crucial matter is whether (7) approximates well the expression in (5): how well does the operator A model the qq̄ eigenstate? The evaluation of ΔE is made most favourable, for given statistics, if the state created from $|0\rangle$ by the operator A has high overlap onto the state $|l\rangle$, as is shown in the next section. The standard use of straight spatial parts in the contour [6, 7], neglects this matter: in contrast, the authors of [8] and [9] used optimised quarkonium operators constructed from a small number of lattice paths. The construction of optimised quarkonium operators for use on the 32^4 lattices is described in the next section.

3. Calculational methods

3.1. The lattices

The constraints limiting a Monte Carlo lattice calculation are largely computational. It is worth discussing this briefly. A reduction of the lattice spacing by a half, whilst maintaining the lattice volume, corresponds to a sixteenfold increase in both the number of lattice points and the numerical processing required for one Monte Carlo sweep. The available computing resources were considerably stretched by the calculations using a 32^4 lattice with the high values of β listed earlier. The Cyber 205 computer at the University of Manchester Regional Computing Centre (UMRCC) provided the necessary processing speed to allow an exploratory study with limited statistics. Numerous techniques were used to exploit its capabilities. These are described at greater length in [11,12], where the details of the equilibrations are also given. A six-hit Metropolis algorithm was used together with the Wilson action. On the basis of a negligible correlation of the expectation value of the Polyakov line between configurations [13], seven configurations at $\beta = 6.29$ were selected as being independent: they all received a minimum of 1550 Monte Carlo sweeps and were separated by at least 200. Similarly, there were eight configurations at $\beta = 6.585$, having had a minimum of 500 sweeps and separated by not less than 200, and six at $\beta = 6.88$ for which the minimum number of sweeps was 750 and the separation greater than 250.

The calculations reported here were mostly performed on the Cyber 205 at UM-RCC. Some additional calculations, using configurations of smaller lattices made available by Teper, were performed on the Cray X-MP/48 at the Rutherford Appleton Laboratory. To analyse the configurations efficiently, the lattice was processed in planes of 32^2 points which greatly reduced the amount of central computer memory used [14]. A typical analysis of a configuration, including the construction of lattices of blocked links (see below) used $\simeq 7$ Mbytes of central memory and $\simeq 800$ Mbytes of disc memory. The calculations were performed using $\simeq 30$ hours of CPU time on the Cyber 205: resources used in the initial generation of the configurations are reported in [12,13].

3.2. Composite links

The normalised autocorrelation function of a lattice operator A at a separation na (where a is the lattice spacing) can be written as

$$\frac{\langle A^{\dagger}(n)A(0)\rangle}{\langle A^{\dagger}(0)A(0)\rangle} = \frac{\sum_i |\langle i|A|0\rangle|^2 (\lambda_i/\lambda_0)^n}{\sum_i |\langle i|A|0\rangle|^2} \rightarrow (\lambda_l/\lambda_0)^n \frac{|\langle l|A|0\rangle|^2}{\sum_i |\langle i|A|0\rangle|^2} \tag{15}$$

where $|i\rangle$ is an eigenstate of the transfer matrix T with eigenvalue λ_i. In the continuum limit T is related to the Hamiltonian H of the continuum theory $(T = \exp(-aH))$. The limit given in (15) is obtained for large enough n: $|l\rangle$ is the highest eigenvalue state with non-zero projection onto the state created out of the vacuum by A. The eigenvalues of T are therefore obtainable from the decay of normalised correlation functions, but preferably at as low a separation n as possible, since the Monte Carlo calculations are eventually swamped by statistical fluctuations at large n. The more the matrix element $\langle l|A|0\rangle$ dominates in the denominator of (15), the better. Where statistics are limited it is, therefore, crucial to use a sensible choice of operator A. Since the number of 32^4 configurations available is small, the construction of optimised operators has been strongly pursued.
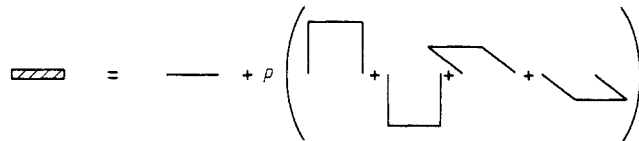

Figure 2. A representation of the basic blocking construction. The straight line segments on the right each represent a single spatial link from the previous level of iteration; p is a constant. The composite link on the left is shaded to indicate spatial blurring.

As the continuum limit is approached the wavefunctions of the gluonic excitations will extend over a greater number of lattice spacings. To achieve an adequate overlap on to such a state it is necessary to use an operator A with a similar degree of spatial correlation. A number of schemes for 'smeared' operator construction have been studied [15,16]; here we use a method similar to 'blocking' (which has been used in studies of pure SU(2) and SU(3) gauge theories on smaller lattices [16]). We use a prescription for replacing the spatial links of a lattice configuration by composite links which have a greater physical extent, but possess the group transformation properties of the original link. The construction involves the lattice paths shown in figure 2, written as

$$W_{\mu}(n) = U_{\mu}(n) + p \sum_{\pm\nu=1,3\neq\mu} U_{\nu}(n)U_{\mu}(n+a\hat{\nu})U_{\nu}^{\dagger}(n+a\hat{\mu}) \tag{16}$$

where $U_\mu(n)$ is a link emanating in direction μ from the point n of the lattice, p is a constant and $U_{-\nu}(n) = U_\nu^\dagger(n - a\hat{\nu})$. The process can be iterated easily to construct composite links of rapidly increasing extent.

To construct a composite link with the greatest spatial blurring the path contributions must be combined on approximately equal terms, so p should be of order unity and blocked and unblocked links should have a similar numerical magnitude. If this were not the case, the next iteration would not combine all five contributions in (16) equally. It is therefore necessary to introduce a normalisation into the blocking procedure. Several methods were considered in [14]: the projection of W_μ onto the 'closest' SU(3) matrix (scheme 1) was used for the $\beta = 6.88$ calculations, and W_μ was divided by a factor $(\text{tr}\, W_\mu W_\mu^\dagger)^{1/2}$ (scheme 2) for $\beta = 6.29$ and 6.585.

Smearing schemes of the type outlined above are used to produce composite links which are then combined together to make quarkonium operators. Following [17], the spatial parts of the quarkonium operators, A_R were constructed from a basis of paths linking points separated by a distance R along a lattice axis. Here, the paths are constructed from blocked links. The two components in the basis were P_1, the straight path between the q and $\bar{\text{q}}$; and P_2, the sum of the four paths displaced one lattice spacing in each spatial direction perpendicular to z. These components are sketched in figure 3. The operator A_R was represented as

$$A_R = P_1 + c_R P_2 \tag{17}$$

and the coefficient c_R selected variationally.
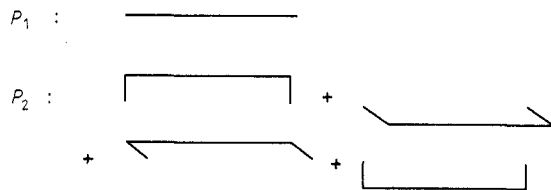
Figure 3. The components P_1 and P_2 forming the variational basis used to construct quarkonium operators (paths are constructed from composite links).

The best smearing scheme maximised the overlaps of candidate operators onto the lattice q$\bar{\text{q}}$ states. It was found [14] that there was little sensitivity in the results to the value of p, all other features of the scheme remaining constant. A value of 0.5 was chosen for the calculations presented here and in [1]. Results were slightly more sensitive to choices of normalisation. Figure 4 shows the behaviour of the approximation to the eigenvalue ratio λ_l/λ_0 inferred from the correlations $\langle A_R^\dagger(n)A_R(0)\rangle/\langle A_R^\dagger(0)A_R(0)\rangle$ at $n = T$ and $T + 1$, for $\beta = 6.88$. Clearly the limit in (15) is achieved for smaller n compared to an A_R constructed from unblocked links [12]. Three blocking iterations at $\beta = 6.88$ gave the best results for R as large as $10a$. The best results at $\beta = 6.29$ and 6.585 were obtained after two blocking iterations: this is in accordance with general expectations since these lattices are coarser than the $\beta = 6.88$ lattice.

The overlaps of the operators A_R which result from the lengthy construction programme outlined above are compared in table 1 with those for the operators S_R consisting of straight paths of unblocked links. This information defines the optimised quarkonium operators. Their autocorrelation at a separation of four lattice spacings is
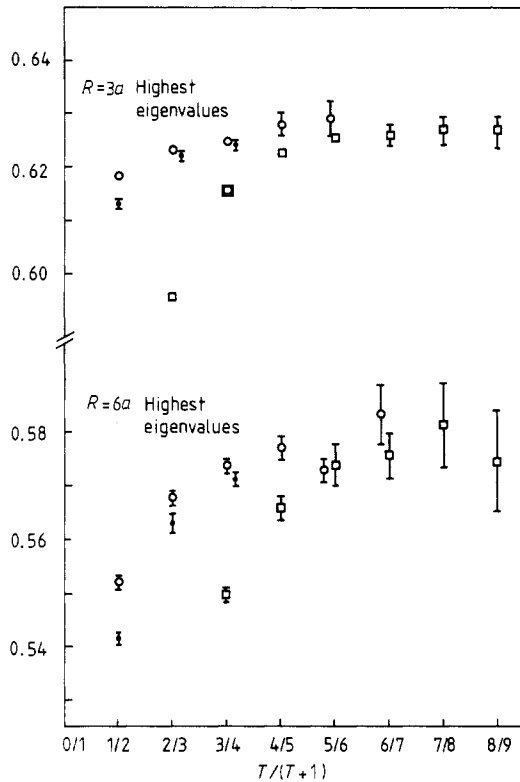
Figure 4. Approximations to the highest ratio, λ_I/λ_0, derived from a comparison of q$\bar{\text{q}}$ operator correlations $\langle A_R^\dagger(T)A_R(0)\rangle$ and $\langle A_R^\dagger(T+1)A_R(0)\rangle$. The behaviour of various models for A_R is shown as a function of T. Open squares, no blocking; full circles, two blockings; open circles, three blockings. The optimised operators at each blocking level are compared: for no blocking, A_R is a straight path of links terminating on fermions (from [12]).

sufficiently dominated by a single mode (see, for instance, figure 4), or at most by two, to allow the extraction of the non-relativistic potential [1].

4. Spin-dependent potentials on the lattice

The main conclusions of previous studies of the spin-dependent potentials on the lattice [7,9] are that V_2, V_3 and V_4 are short-range potentials whilst V_1 is long range. One of the aims of the present study was to discover whether this same picture emerges from a lattice calculation deeper into the continuum limit. The finer spacing of the lattice points should make clearer the short-range structure of the potentials. This is especially important when considering the scalar spin–spin potential, which is proportional to a δ function in continuum perturbation theory.

The potentials V_{1-4} were evaluated using the 32^4 lattice configurations and the optimised quarkonium operators described in the previous section. The programs were also run on sequences of 16^4 configurations at $\beta = 6.0$ and 20^4 configurations at $\beta = 6.2$, generated according to a Metropolis algorithm with the Wilson action

Table 1. Values of the coefficients c_R specifying the smeared operator A_R according to (17). The basis paths are constructed from composite links at the second blocking level for $\beta = 6.29$ and 6.585, and at the third level for $\beta = 6.88$. A comparison of the matrix elements of A_R and S_R between the vacuum and the q$\bar{\text{q}}$ state at separation R along a lattice axis is also given, where S_R is a straight path operator constructed from unblocked links.

β	R/a	c_R	$|\langle q\bar{q}|A_R|0\rangle|^2$	$|\langle q\bar{q}|S_R|0\rangle|^2$
6.29	1	3.0	0.96	
	2	−2.4	0.89	0.61
	3	−2.1	0.80	0.40
	4	−2.1	0.73	0.25
	5	−2.2	0.60	0.16
	6	−2.4	0.52	0.10
	7	−2.5	0.45	0.06
	8	−2.8	0.38	0.04
	9	−3.1	0.32	0.03
	10	−3.4	0.26	0.01
6.585	1	8.43	0.96	
	2	−2.2	0.91	0.63
	3	−2.0	0.84	0.42
	4	−2.0	0.76	0.27
	5	−2.1	0.67	0.17
	6	−2.2	0.60	0.11
	7	−2.3	0.52	0.06
	8	−2.4	0.43	0.04
	9	−2.5	0.36	0.03
	10	−2.7	0.30	0.02
6.88	1	4.9	0.99	
	2	−0.49	0.97	0.64
	3	−0.46	0.93	0.44
	4	−0.45	0.90	0.30
	5	−0.45	0.85	0.19
	6	−0.46	0.81	0.13
	7	−0.47	0.77	0.09
	8	−0.48	0.72	0.05
	9	−0.49	0.68	0.04
	10	−0.51	0.64	0.03

by Teper. 60 configurations, each separated by 25 sweeps, at $\beta = 6.0$ were analysed, and 12 at $\beta = 6.2$ also separated by 25 sweeps. Optimised quarkonium operators for these additional lattices were required. A brief study was made of blocking levels and variational combinations of paths at $\beta = 6.0$ with the result that twice-blocked, scheme 2 normalised spatial links were used. The combinations of P_1 and P_2 paths for various R were similar to those at $\beta = 6.29$ shown in table 1. Since there seemed to be little β dependence between 6.0 and 6.29, this same prescription was chosen for $\beta = 6.2$.

The lattice representations $F_{\mu\nu}^{L}$ of the chromoelectric and chromomagnetic fields are based upon the combination $(1/2i)(P_{\mu\nu}(n) - P_{\mu\nu}^{\dagger}(n))$ where $P_{\mu\nu}$ is the plaquette operator:

$$a^2 g F_{\mu\nu}^{L}(n) = \frac{(1/2i)(P_{\mu\nu}(n) - P_{\mu\nu}^{\dagger}(n))}{\langle \frac{1}{3} \text{Re}\,(\text{tr}\,P_{\mu\nu})\rangle}. \tag{18}$$

The division by the average plaquette is an attempt to cancel away $O(a^4)$ terms appearing in the numerator [9]. At the values of β studied here the naive lattice

potentials (calculated using only the numerator of the RHS of (18)) are increased due to this normalisation by factors of 2.59, 2.41 and 2.27 at $\beta = 6.29$, 6.585 and 6.88 respectively. The results presented here include these factors. The $F^L_{\mu\nu}$ (loosely referred to below as colour fields) are represented by the normalised combination of links shown in figure 5. The symmetric combinations should represent more accurately the colour field at the lattice position required, shown as a cross. The electric field operator involves time-directed links and it is taken to represent the electric field at the *centre* of a link.


Figure 5. Lattice structures used to represent chromomagnetic (top) and chromoelectric (bottom) field operators. The combinations are considered to represent the field at the lattice position marked with a cross.

4.1. Spin–spin potentials, and the A_{1u} hybrid state

We have evaluated the expectation values of loops with the plaquette-like operators shown in figure 5 inserted at points along the timelike sections; figure 6 is typical. The temporal length τ was taken to be $5a$, which from studies of the quarkonium operators [1] is more than large enough for (7) to be an accurate representation of (5). The integrals over t in (10,11,13,14) were approximated by sums. The advantages of small τ (in terms of reduced computational effort and accuracy of evaluation) have to be balanced against the need to evaluate colour field correlations for as great a separation t as possible. An analysis with $\tau = 6a$ found no dependence upon τ in the resulting spin potentials, although the statistical errors were higher. The calculation with $\tau = 5a$ limited the evaluation of chromomagnetic field correlations to those with separations t only as great as $3a$.
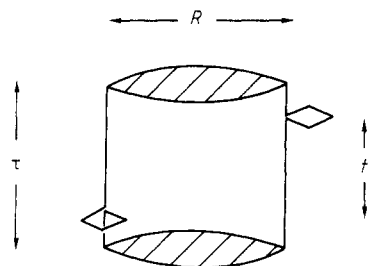
Figure 6. Example loop used to evaluate the spin–spin potentials. The representation in figure 5 of B^L is inserted twice into the generic structure in figure 1 to yield a sum of gauge invariant objects. R is the separation of the q and $\bar{q}$, τ is the temporal extent of the contour, and t is the temporal separation of the colour field insertions.

The time-directed links (except for those which are part of the chromoelectric field operators) were replaced in the calculation by multihit (MH) links [18,19], implemented following [19]. This procedure reduces the statistical fluctuation of the link (and of loops containing it) over a set of independent configurations. This reduced errors by about 20%, not as great an improvement as has been obtained for smaller β (e.g. [19]). This is to be expected since the physical volume of the lattice which contributes to the link averaging becomes smaller as β increases.

The procedure for the completion of the integrals uses the $\exp(-\Delta E't)$ behaviour of the colour field correlations, where $\Delta E'$ is the energy difference between the $q\bar{q}$ ground state and the lowest state excited from it by a colour field operator. For $\langle B_x^L(t)B_x^L(0)\rangle_C$ correlations, this is the E_u hybrid (studied in [1,2]) and for the $\langle B_z^L(t)B_z^L(0)\rangle_C$ it is the A_{1u}. This can be determined from the symmetries of the states. It was possible to determine reasonably well the A_{1u} energy from some of the $\langle B_z^L B_z^L\rangle_C$ correlations, but otherwise the previously determined E_u energies [1] were used (given in the appendix), and the A_{1u} energies were estimated from the falloff in the $\langle B_z^L B_z^L\rangle_C$ correlations between $t = 2a$ and $3a$. The integrals were then completed analytically.
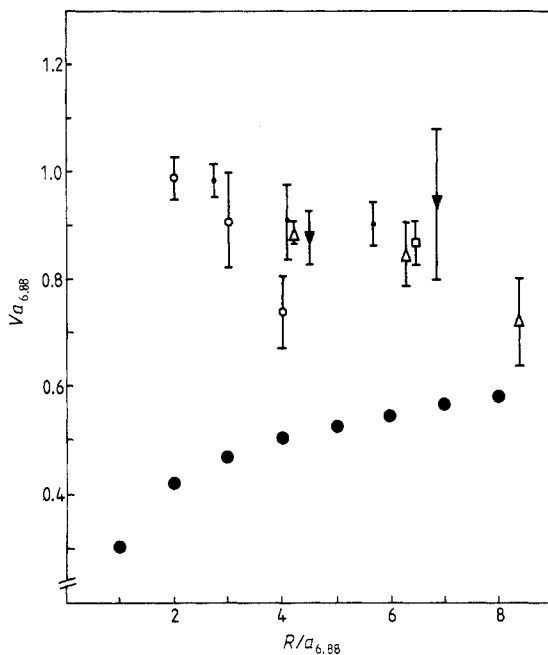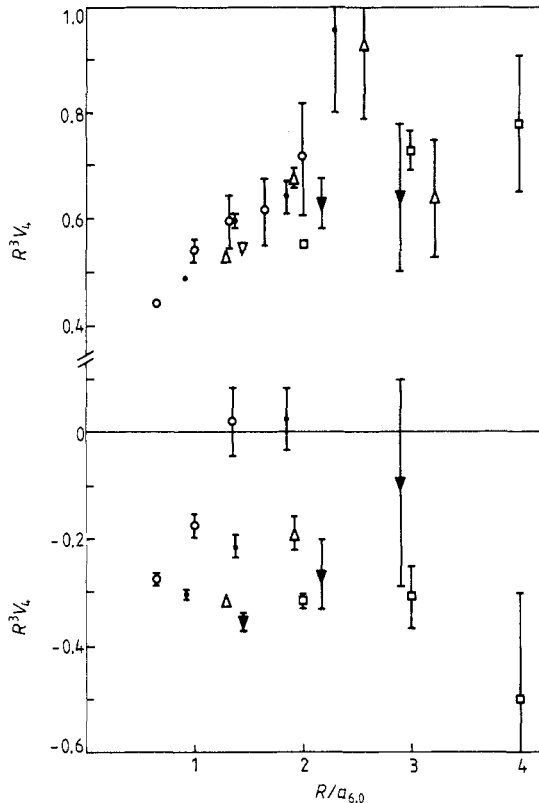

Figure 7. Results for the A_{1u} potential for $q\bar{q}$ separation R at various β (for key, see caption to figure 8) together with the A_{1g} potential at $\beta = 6.88$, shown as full circles. The calculations have been rescaled according to an assumed asymptotic dependence of the lattice spacing a upon β to form a single plot.

Finally we examined the dependence of the expectation value of the loops upon the absolute positions of the colour field insertions, rather than upon their relative positions. It was concluded that any such dependence in the data was small enough to be hidden within the statistical errors, and an average over absolute positions of the insertions was taken.

In the general behaviour of the correlations there is a correspondence with perturbative results based on one gluon exchange, as noted by [8]. In particular there

seems to be in some cases a change in sign of the $\langle B_x^L B_x^L \rangle_C$ correlations for large t. In contrast, the $\langle B_z^L B_z^L \rangle_C$ correlations fall monotonically and for some values of R are remarkably close to a single exponential decay between $t = a$ and $3a$. This allows an estimation of the non-relativistic potential of the A_{1u} hybrid state. The results are displayed on a single plot, figure 7, assuming asymptotic scaling. The $\beta = 6.88$ A_{1g} potential [1] is shown for comparison. The reasonable agreement between the results at different β suggests that an approximate form of asymptotic scaling is being obeyed by this lattice quantity. When compared to the E_u potential [1] there is evidence that the A_{1u} potential is lower, especially away from the origin. However, the way in which the A_{1u} potential has been evaluated can lead to an underestimation, whereas the method used in [1] to calculate the E_u potential is more likely to produce an overestimate.

Figure 8. Lattice results for the scalar (V_4) and tensor (V_3) spin–spin potentials in q$\bar{\text{q}}$, given in dimensionless form. A single plot has been obtained by rescaling the lattice spacings at each β, as in figure 7. Results at $\beta = 6.0$ were obtained from a 16^4 lattice, at $\beta = 6.2$ from a 20^4 lattice and the remainder on 32^4 lattices. Open squares, $\beta = 6.0$; inverted full triangle, $\beta = 6.2$; open triangle, $\beta = 6.29$; full circle, $\beta = 6.585$; open circle, $\beta = 6.88$.

The $\langle B_i^L B_i^L \rangle$ correlations were combined into the spin–spin potentials V_3 and V_4 according to (10) and (11) and the extrapolation procedure given above. The results are listed in table 2 and the extrapolated potentials (after a rescaling of R according to asymptotic β dependence of a) are shown in figure 8. The rescaling of R only introduces a small inaccuracy in the abscissae of the plotted points. The use of dimensionless quantities as the ordinates eliminates any error in the vertical direction
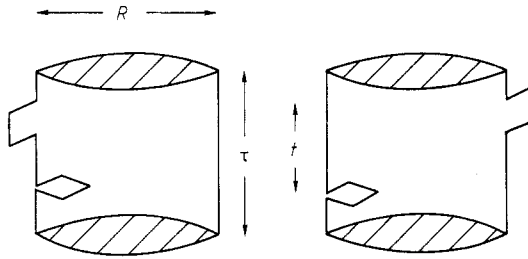
Figure 9. Examples of loops used to evaluate V_1 (on the left) and V_2 (on the right). The upper insertion arises from a chromoelectric field operator and the lower one arises from a chromomagnetic field operator.

due to deviations from asymptotic scaling. It is possible to put physical units on the R axis by assuming that the lattice prediction for the string tension is equal to that used in continuum models of heavy quarkonia. We have $a(\beta = 6.585) \simeq 0.066$ fm, and the points for $\beta = 6.585$ in the figure are at $R = 2a, 3a$ etc. After the calculation of the spin–orbit potentials has been described, these plots will be discussed further.

Table 2. V_3 and V_4 potentials for various R and β. V_i^t corresponds to the truncated range of integration ($|t| \leq 3a$) in (10) and (11); V_i^e includes a contribution from an extrapolation of the integrals. V_4^{pert} is the perturbative evaluation of the scalar spin–spin potential to order $1/\beta$. The results are multiplied by 10^4 and the errors are statistical.

β	R/a	$a^3 V_3^t$	$a^3 V_3^e$	$-a^3 V_4^t$	$-a^3 V_4^e$	$-a^3 V_4^{\text{pert}}$	$-a^3(V_4^e - V_4^{\text{pert}})$
6.0	2	686(7)	687(10)	441(13)	398(16)	302	96(16)
	3	257(13)	270(14)	128(21)	114(21)	73	41(21)
	4	113(21)	122(21)	75(32)	78(32)	23	55(32)
6.2	2	664(7)	681(8)	473(17)	445(19)	292	153(19)
	3	223(16)	233(18)	109(20)	99(24)	71	28(24)
	4	77(19)	100(23)	23(30)	15(30)	26	−11(30)
	5	46(21)	55(23)				
6.29	2	650(4)	666(6)	431(6)	391(12)	287	104(12)
	3	232(5)	251(7)	96(8)	70(11)	70	0(11)
	4	107(7)	146(22)	23(11)	14(25)	22	−8(30)
	5	50(9)	51(9)				
	6	44(13)	59(14)				
6.585	2	595(3)	609(5)	416(4)	382(10)	274	108(10)
	3	203(4)	221(6)	100(6)	79(8)	67	12(8)
	4	86(4)	100(5)	18(7)	4(9)	21	−17(9)
	5	47(5)	76(12)				
6.88	2	543(3)	553(5)	390(4)	344(13)	262	82(13)
	3	183(3)	201(7)	90(6)	64(8)	64	0(8)
	4	75(4)	93(8)	21(7)	3(10)	20	−17(10)
	5	44(4)	49(5)				
	6	30(5)	33(5)				

4.2. Spin–orbit potentials

In this section the calculation of the spin–orbit potentials V_1 and V_2 is described. Using a temporal extent of $\tau = 5a$ for loops such as figure 9, the correlations

$\langle B_x^{\mathrm{L}}(0)E_y^{\mathrm{L}}(t)\rangle_{\mathrm{C}}/\langle 1\rangle_{\mathrm{C}}$ were calculated for $t = a/2$, $3a/2$ and $5a/2$. The factors of t in the integrands in (13) and (14) make the extrapolation of the integration range to infinity more difficult than before. We assume exponential decay of the correlations according to $\exp(-\Delta E' t)$ for $|t|\rangle 5a/2$, where $\Delta E'$ is the difference between the non-relativistic energies of the E_u and the A_{1g} states.

Table 3. Derivatives of the V_1 and V_2 spin–orbit potentials multiplied by 10^4 for various β and R, together with statistical errors. $V_i^{\prime t}$ is the truncated result involving an integration range in (13) and (14) of $-5a/2 \leq t \leq 5a/2$, whilst $V_i^{\prime e}$ includes an inferred contribution from the rest of the integration range.

| β	R/a	$a^2 V_2^{\prime t}$	$a^2 V_2^{\prime e}$	$-a^2 V_1^{\prime t}$	$-a^2 V_1^{\prime e}$
6.0	2	459(9)	651(40)	229(8)	306(20)
	3	147(15)	240(26)	196(15)	281(25)
	4	33(26)	68(30)	146(22)	223(28)
6.2	2	416(9)	525(21)	176(6)	218(12)
	3	153(12)	209(16)	169(12)	225(15)
	4	57(17)	96(20)	161(20)	234(25)
	5	11(32)	13(32)	135(27)	187(29)
6.29	2	395(4)	522(30)	149(3)	186(12)
	3	146(6)	214(12)	132(5)	171(12)
	4	60(8)	104(13)	113(7)	144(12)
	5	18(11)	19(11)	127(10)	179(14)
	6			116(15)	175(17)
	7			125(23)	204(32)
	8			111(29)	189(36)
6.585	2	358(3)	476(20)	111(2)	140(8)
	3	124(4)	194(16)	91(3)	121(8)
	4	48(5)	82(12)	75(5)	98(7)
	5	35(6)	66(10)	74(6)	99(9)
	6	12(8)	28(10)	69(8)	92(10)
	7			63(10)	78(11)
	8			51(13)	43(15)
6.88	2	328(3)	514(40)	82(2)	121(10)
	3	108(3)	210(20)	63(3)	99(10)
	4	41(4)	89(12)	57(4)	95(12)
	5	16(6)	35(8)	54(5)	87(10)
	6	12(7)	30(9)	56(9)	100(14)
	7			42(7)	68(9)
	8			44(8)	69(10)

The correlations were used to produce the derivatives of the V_1 and V_2 potentials listed in table 3. The estimates $V_i^{\prime t}$ come from the integrals in (13) and (14) truncated at $t = 5a/2$ and $V_i^{\prime e}$ includes an inferred contribution from the rest of the t interval. Clearly, the relative contributions from the extrapolation interval are quite important and to include the errors which might arise from the extrapolation procedure the quoted uncertainties in the results $V_{1,2}^{\prime e}$ have been increased.

The extrapolated values $V_1^{\prime e}$ (henceforth the label e is dropped) in table 3 are normalised by the string tension K calculated in [1] and plotted in figure 10 against separation R rescaled according to asymptotic β-dependence of a. (The value of K for $\beta = 6.0$ is taken from [20] and for $\beta = 6.2$ from [21]). Clearly, V_1 is a long-range potential, which supports the calculations reported in [7,9] but not those in [6].
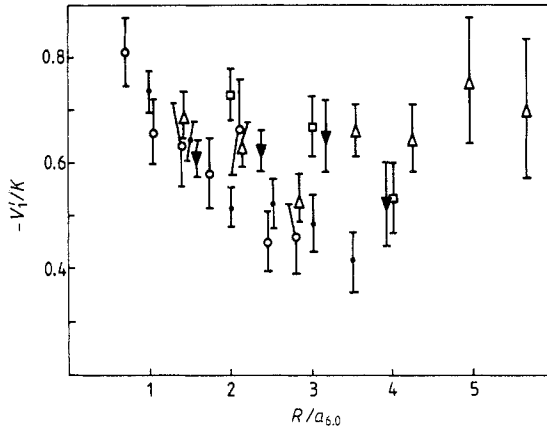
Figure 10. Lattice results for the derivative of the spin–orbit potential V_1, normalised by the string tension K. Symbols as in figure 8. The separations R at each β have been rescaled according to the expected asymptotic behaviour.

The results when normalised by the string tension are consistent with β-independence (general scaling).
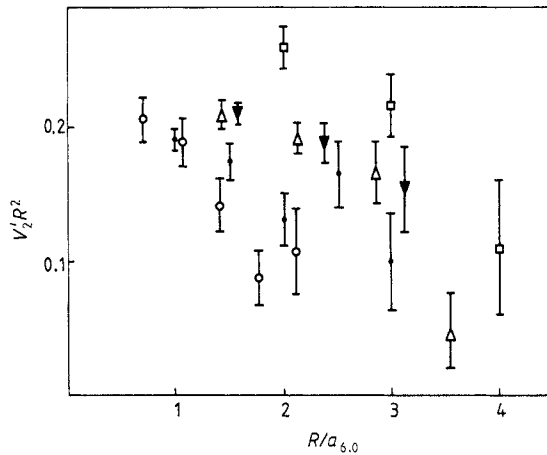
Figure 11. Lattice results for the derivative of the spin–orbit potential V_2, given as the dimensionless $V_2' R^2$. R rescaled as in figure 10 and symbols as in figure 8.

Figure 11 gives the results for the derivative of V_2. Again the extrapolated values in table 3 are taken, the dimensionless $V_2' R^2$ is plotted, and R rescaled. It is important to check whether Gromes' relation [22] is satisfied. This analytic result relating the two spin–orbit potentials and the non-relativistic potential V_0 is

$$V_0 = V_2 - V_1. \tag{19}$$

For the results at $\beta = 6.29$, 6.585 and 6.88 (using the non-relativistic potential V_0 calculated in [1]) the RHS of (19) is too small. This is likely to be due to the normalisation of the chromoelectric field operators used here. If the procedure in [9] is correct, then the normalisation used here will cause deviations from (19) which

are different for different R. Essentially, the procedure fails to remove self-energy contributions from the chromoelectric field operators in the environment of a Wilson loop [9]. The errors are the same in $V_1'(R)$ and $V_2'(R)$ and so it should be possible to rescale the two so that (19) is satisfied. By necessity, the rescaling factor is different for different R and β. The rescaled values of V_1' are plotted in figure 12. For large R V_2' is very small and the rescaling simply puts $-V_1'/K$ equal to one ($V_0' \simeq K$ for large R) but the points in figure 12 are consistent with this value over a range of R below about 0.4 fm, which is not large. The rescaled V_2' are shown in figure 13 and suggest a $1/R^2$ behaviour. The significance of these results, and of those for the spin–spin potentials, is examined next.
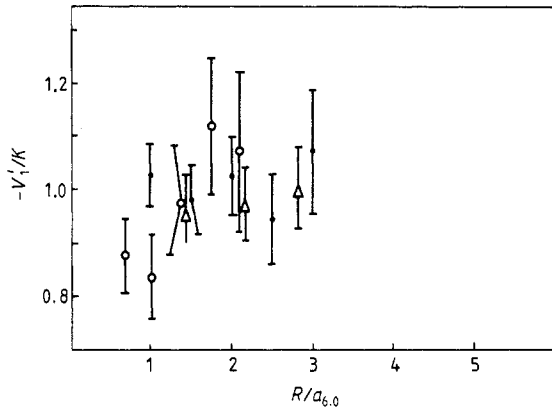

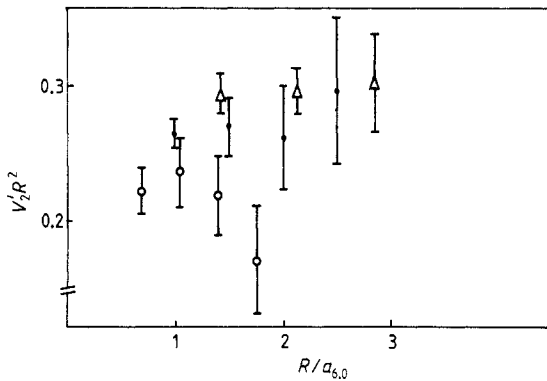**Figure 12.** As figure 10 but for rescaled V_1'.

Figure 13. As figure 11 but for rescaled V_2'.

4.3. Interpretation of the results

The $O(1/m_q^2)$ corrections to the non-relativistic potential between q and $\bar{q}$ are important not only for calculating the spectrum of quarkonia, but also for clarifying the fundamental nature of the q$\bar{q}$ interaction at hadronic length scales. The interaction at

such length scales can be represented in terms of forces due to the effective exchange of particles of various Lorentz characters and then Bethe–Salpeter methods used to deduce the $q\bar{q}$ Hamiltonian in an expansion in $(1/m_q)$ [23]. Scalar and vector type interactions contribute to the m_q-independent term, the non-relativistic potential V_0 and the relative contributions can be clarified by examining the $O(1/m_q^2)$ terms in the Hamiltonian. Neglecting any P,A or T interaction, the potentials V_{0-4} can be written:

$$V_0 = \epsilon + S \qquad V_1' = -S' \qquad V_2' = \epsilon' \qquad V_3 = \epsilon'/R - \epsilon'' \qquad V_4 = 2\nabla^2\epsilon \qquad (20)$$

where ϵ is the vector and S the scalar contribution to V_0. The standard expression for V_0, to which the calculations in [1] were fitted, is

$$V_0 = (A/R) + KR + C \qquad (21)$$

with A,K and C listed in [1] for each β on the 32^4 lattice. Thus S and ϵ can be represented by

$$\begin{aligned}
\epsilon(R) &= (1-\eta)(A/R) + (1-\gamma)KR \\
S(R) &= \eta(A/R) + \gamma KR
\end{aligned} \qquad (22)$$

where η and γ are constants. Hence

$$\begin{aligned}
\frac{-V_1'}{K} &= -\eta\frac{A}{KR^2} + \gamma \\
V_2'R^2 &= -(1-\eta)A + (1-\gamma)KR^2 \\
V_3R^3 &= -3(1-\eta)A + (1-\gamma)KR^2 \\
V_4R^3 &= 4(1-\gamma)KR^2 - (1-\eta)4\pi AR^3\delta^3(R).
\end{aligned} \qquad (23)$$

At a separation R of two lattice spacings at $\beta = 6.29$ the value of $-(A/KR^2)$ is 2.69. Therefore the values of $-V_1'/K$ in figure 12 imply that η is very small (≤ 0.01) and that γ is close to one. This assignment is supported by figure 13 where the points agree very well with the choice $\eta = 0$ and $\gamma = 1$. The calculated values of V_3 in figure 8 are generally smaller than those to be expected from (23) but this is likely to be an inaccuracy in the plaquette normalisation of the colour field operators. We have evidence, therefore, that the $q\bar{q}$ interaction divides neatly into a Coulomb-like vector interaction and a linear scalar part. We conclude firstly that the (scalar) Lüscher contribution of $-(\pi/12R)$ to the non-relativistic potential is absent in the range of R studied. The Coulomb-like part of V_0 appears to be purely vector in origin, so the correspondence between $-(\pi/12)$ and the values of A in [1] seems to be a coincidence. The Lüscher term may contribute to the potential at values of R larger than those studied here: indeed its derivation is specifically for large R. Secondly, we conclude that the calculations support the string picture of long-range chromoelectric fields confining the q and $\bar{q}$, which has been shown to give a scalar linear potential [25].

Since the results for V_1', V_2' and V_3 in figures 8,12 and 13 are generally consistent with universal curves regardless of β, approximate continuum results are being generated. The exception is the scalar spin–spin potential V_4 in figure 8 and table 2. The preferred dependence of the results upon R/a rather than upon the rescaled R suggests that substantial perturbative lattice contributions (proportional to inverse powers of β) are present. Lattice calculations are made in the hope that these lattice artifacts are not

large enough in the range of β studied to mask a component scaling asymptotically. If the expected continuum result is small, then there is likely to be a problem. Away from the origin V_4 is expected to be close to zero, so we need to consider the perturbative lattice artifacts. These have been calculated to $O(1/\beta)$ using the lattice perturbative methods outlined in [9]. The calculation is specific to the choice of colour field operators used in this study. The results are listed in table 2. The lattice estimates of V_4 minus the $O(1/\beta)$ perturbative contributions are also given. Even taking into account the errors, it seems that for $R > 2a$ the Monte Carlo results are consistent with the $O(1/\beta)$ perturbative artifacts. For $R = 2a$, the residue is likely to be due to perturbative artifacts in $O(1/\beta^2)$ or above. There is no strong evidence in the lattice results that the V_4 potential differs from zero for the range of distances examined.

5. Conclusions

In this paper the spin-dependence to $O(1/m_q^2)$ of the potential between a heavy quark and antiquark has been investigated on large lattices and in pure QCD using the non-perturbative formalism of [5]. We have used complicated lattice operators as models for the heavy q$\bar{\text{q}}$ state. They were constructed according to intuitive ideas concerning the arrangement in space of the gluonic field in quarkonium, and prescriptions for their structure have been given. The operators were used previously [1] to calculate non-relativistic potentials for the A_{1g} state of heavy quarkonium.

The results on the 32^4 lattices confirm several features of the spin-dependent potentials. It now seems clear that the only potential whose behaviour, in the range of R studied, is not consistent with perturbation theory is the 'same-side' spin–orbit potential V_1. The results for the scalar spin–spin potential V_4 are disappointing since its behaviour very close to the origin remains unresolved.

It has been possible using the results obtained here and in [1], to demonstrate an important consistency between fits to the non-relativistic potential V_0 and to the (rescaled) spin–orbit potentials. The standard separation of V_0 into a Coulomb-like and a linear part seems to be more than a convenient parametrisation; the evidence is that each term has a distinct Lorentz character which is revealed in the spin-dependent corrections. Within the usual range of uncertainty inherent in a Monte Carlo study, the Coulomb-like term seems to be wholly vector in nature, whilst the linear term seems to be wholly scalar. The small values of the lattice spacings attainable on a 32^4 lattice, and hence the detail in the calculation, are instrumental in reaching this conclusion.

The calculation of the A_{1u} non-relativistic q$\bar{\text{q}}$ potential given here, it is believed, for the first time in any detail, indicates a behaviour similar to the E_u potential. This is surprising if the q$\bar{\text{q}}$ state is viewed as a quantised string. The E_u state in this picture would contain a single string phonon whilst the A_{1u} would possess three and have a higher energy.

The 32^4 lattices have imposed considerable computational difficulties which have been overcome through a careful allocation of the available resources. The manipulation of large configurations and the improvement of lattice operators have been given great attention. A remaining obstacle to the extension of lattice calculations further into the continuum limit is the phenomenon of critical slowing down. A solution to this problem is required before studies very much more ambitious than the one described here can be undertaken.
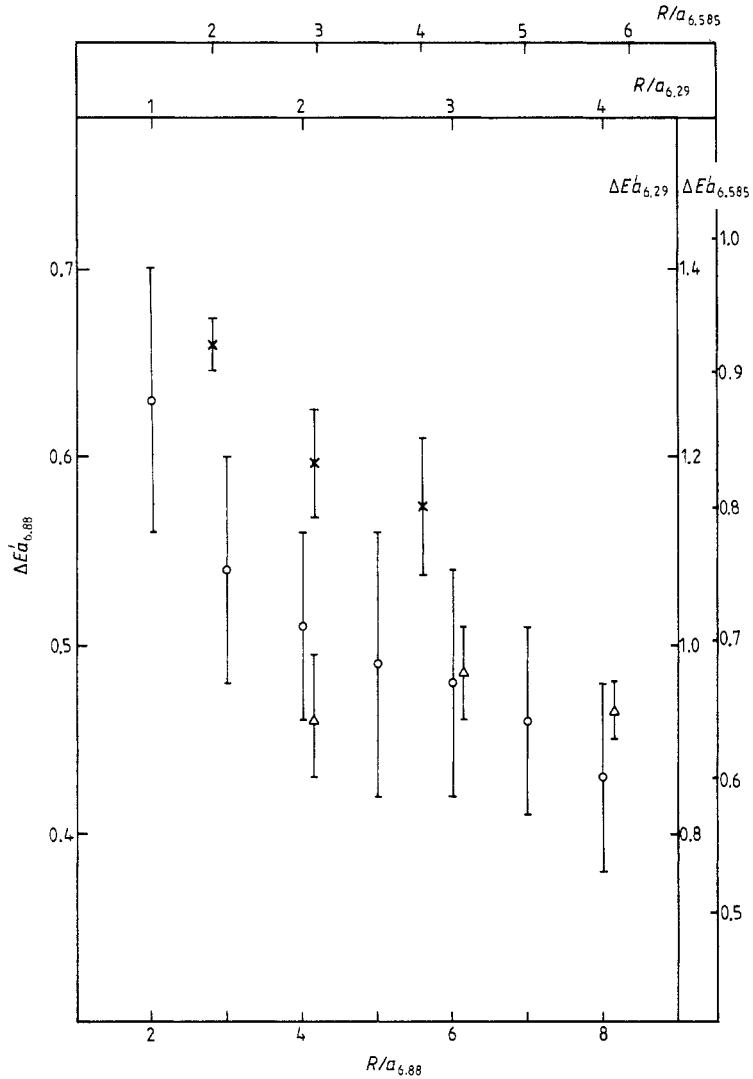
Figure 14. Differences $\Delta E'$ between the E_u and A_{1g} potentials in q$\bar{\text{q}}$, for various separations which have been rescaled according to asymptotic behaviour.

Acknowledgments

Appendix

For completeness, the calculated differences in energy between the E_u hybrid and A_{1g} ground states of q$\bar{\text{q}}$ for various separations can be extracted from the information given

in figure 14. The separations R are along axes of the 32^4 lattices at $\beta = 6.29$, 6.585 and 6.88. The axes of the plot have been scaled according to an assumed two-loop asymptotic behaviour. The $\beta = 6.88$ E_u potential was reported briefly in [1].

References

[1]   Ford I J, Dalitz R H and Hoek J 1988 *Phys. Lett.* **208B** 286
[2]   Hasenfratz A and Hasenfratz P 1985 *Florida preprint* FSU-SCRI-85-2
       Kogut J B 1979 *Rev. Mod. Phys.* **51** 659; 1983 *Rev. Mod. Phys.* **55** 775
[3]   Griffiths L A, Michael C and Rakow P E L 1983 *Phys. Lett.* **129B** 351
[4]   Isgur N and Paton J 1983 *Phys. Lett.* **124B** 247; 1985 *Phys. Rev.* D **31** 2910
[5]   Eichten E and Feinberg F 1981 *Phys. Rev.* D **23** 2724
[6]   de Forcrand P and Stack J D 1985 *Phys. Rev. Lett.* **55** 1254
[7]   Campostrini M, Moriarty K J M and Rebbi C 1986 *Phys. Rev. Lett.* **57** 44; 1987 *Phys. Rev.* D **36** 3450
[8]   Michael C Rakow P E L 1985 *Nucl. Phys.* B **256** 640
[9]   Huntley and Michael C 1987 *Nucl. Phys.* B **286** 211
[10]   Fukugita M 1987 *Lectures presented at the Symposium/Workshop on Lattice Gauge Theory using Parallel Processors (1987) Beijing, China; Yukawa Hall Kyoto preprint* RIFP-703
[11]   Bunk B and Sommer R 1986 *Comp. Phys. Commun.* **40** 229
[12]   Hoek J 1987 *Z. Phys.* C **35** 369
[13]   Hoek J and Dalitz R H 1986 *Phys. Lett.* **177B** 180
[14]   Ford I J 1987 *DPhil thesis* Oxford University
[15]   Albanese M *et al* 1987 (The APE collaboration) *Phys. Lett.* **192B** 163
[16]   Teper M 1987 *Phys. Lett.* **183B** 345; **185B** 121
[17]   Huntley A and Michael C 1986 *Nucl. Phys.* B **270** 123
[18]   Parisi G, Petronzio P and Rapuano F 1983 *Phys. Lett.* **128B** 418
[19]   de Forcrand P and Roiesnel C 1985 *Phys. Lett.* **151B** 78
[20]   de Forcrand P, Schierholz G, Schneider H and Teper M 1985 *Phys. Lett.* **160B** 137
[21]   Barkai D, Moriarty K J M and Rebbi C 1984 *Phys. Rev.* D **30** 1293
[22]   Gromes D 1984 *Z. Phys.* C **26** 401; 1987 *Heidelberg preprint* HD-THEP-87-16
[23]   Gromes D 1977 *Nucl. Phys.* B **131** 80
       Stroscio M A 1975 *Phys. Rep.* **22C** 215
[24]   Lüscher M 1981 *Nucl.Phys.* B **180** 317
[25]   Buchmüller W 1982 *Phys. Lett.* **B112** 479